Dissociation dynamics of HD^+ in intense femtosecond laser pulses by one-dimensional wave-packet propagation

Rangana Bhattacharya and S. S. Bhattacharyya

Department of Materials Science, Atomic and Molecular Physics Section, Indian Association for the Cultivation of Science, Jadavpur, Kolkata 700032, India

(Received 30 September 2008; revised manuscript received 29 November 2008; published 20 April 2009)

Dissociation of HD^+ molecular ion by intense femtosecond laser pulses is studied theoretically using quantum propagation of nuclear vibrational wave packets. Radiative pulses of peak intensity in the range of 10^{14}–10^{15} W/cm^2 with carrier wavelength of 800 nm are applied on the system. In our calculation we have used a four component wave packet in two spatial regions for studying the dynamics of dissociated fragments and the nondissociated molecules simultaneously. This technique enables us to investigate the dynamics by varying the pulse duration (15–75 fs) and the peak amplitude of the field for the initial vibrational state $\nu_i = 0$. The effect of permanent dipole moments and nonadiabatic mixing coefficients of the system on dissociation probability and the branching ratio of photofragments between two outgoing channels are also discussed. Studies of kinetic energy spectra help us to estimate the number of photon absorption and shift of the field induced resonances from the field free levels. The dissociation spectrum at high intensity has been compared with available experimental results.

DOI: 10.1103/PhysRevA.79.043415 PACS number(s): 33.80.Gj, 42.50.Hz, 33.80.Wz

I. INTRODUCTION

Study of behavior of the simplest molecules in intense laser fields began in earnest in the late 1980s and early 1990s. It was soon discovered that the nonperturbative interaction of both the electronic and nuclear degrees of freedom with the incident light, and their interplay, can lead to a rich set of phenomena. In two pioneering papers He and coworkers [1,2] indicated the importance of above threshold dissociation channels through time-independent nonperturbative calculations. Further work led to the understanding of bond-softening, vibrational trapping [3], laser induced alignment [4], and zero photon dissociation [5] processes. The early workers could focus on some very general features of molecular dynamics related to fundamental issues in laser-molecule interaction through study of the simplest species H_2^+. A review of basic processes involved in strong field dissociations was made in 1995 [6]. A brief discussion of the works in this field up to 1996 was given by Datta *et al.* [7].

Also, parallel advances in the generation and control of ultrashort and ultraintense laser pulses triggered searches for specific phenomena where the large intensity and its rapid variation (within the time scale of nuclear motion) play crucial roles. The simulation of the molecular dynamics with pulses containing only a few cycles and with intensities of the order of 10^{14}–10^{15} W/cm^2, mainly in the near-ir range, is now a very active area of laser science. A thorough review of the laser-molecule interactions, particularly for H_2^+, with a discussion of the physics involved, can be found in [8]. However, in each case, even rough estimates of the main features of a process require detailed computation of the evolution of the molecular states under specific conditions. Taking advantage of the very different time scales of the electronic and nuclear motions (in the attosecond and femtosecond regimes, respectively), many workers invoked the Born-Oppenheimer (BO) separation of the electronic and nuclear degrees of freedom to understand the dissociative multiphoton processes that may occur. The principles underlying this approach were discussed in detail in [9]. In his review Posthumus [8] interpreted the salient features of the experimental results in terms of the electronic potential energy surfaces. It was also shown that for ir excitations of H_2^+, the electronic Born-Oppenheimer basis may be limited to the ground $1s\sigma_g$ and the next dissociative electronic state $2p\sigma_u$ if the field molecule interactions are taken in length gauge [10]. Early works of Jolicard and Atabek [11] derived and physically explained the positions, widths, shifts, and relative heights of kinetic energy peaks of protons due to multiphoton dissociation of H_2^+ by femtosecond pulses within this framework. In recent work this two-state model has been used by Lefebvre *et al.* [12] to find the parameters for effective control of dissociation of H_2^+ and a very detailed study of dissociation of H_2^+ by femtosecond ir pulse has been made by Peng *et al.* [13] within the same manifold of electronic states.

Authors going beyond the Born-Oppenheimer separation at first used a collinear model of the electronic structure of H_2^+ to investigate the relative importance of ionization and dissociation from a vibrationally excited state [14]. More recent calculation on H_2^+ by Rotenberg *et al.* [15] has also concentrated on the influence of nuclear motion (treated classically). Similar electronic structure model of H_2^+ has also been adopted to illustrate dynamical effects when both ionization and dissociation occur [16]. For H_2^+ and D_2^+ Serov *et al.* [17] used the multidimensional time-dependent wave-packet propagation for detailed comparisons of the angle-resolved dissociation probability with experiments in which H_2^+ was prepared by electric discharge.

More recently, the polar one electron diatomic molecule HD^+ has also become the focus of interest. It was shown that the breaking of the g-u symmetry in HD^+ and its attendant presence of permanent dipole moments could be used for controlling the angular distribution of the dissociation products [18]. Further, the resonant nature of the ir photon ab-

sorption can lead to very interesting changes in the line shapes and branching ratios [19].

However, studies on the dynamics of fragmentation of HD^+, in short intense pulses in detail comparable to that for H_2^+, have started only very recently. Roudnev *et al.* [20–22], in a series of papers, computed the propagation of the electronuclear wave packet for conditions where pure dissociation and dissociative ionization compete. They used both a linear model in which the motion of the electron can take place only along the direction of the molecular axis (aligned along the direction of polarization) and also a nonlinear structure model in which the electron can be away from the axis and must be described in a cylindrical coordinate system. Pulses with different durations and peak intensities were employed. As the peak intensity is increased, keeping the shape of the pulse constant, the importance of ionization steadily increases.

In spite of all these advances the predictive power of the computation intensive eletronuclear wave-packet propagation seems to be rather limited because different models of electronic structure may give very different results. On the other hand, a lot of understanding can still be obtained by the study of the dissociative decay of the nuclei on the coupled Born-Oppenheimer potential surfaces for conditions where ionization is not significant, as the work of Peng *et al.* [13] for H_2^+ amply demonstrates.

In the present work we concentrate on the dissociation mechanism and the distribution of the fragments of HD^+ for very intense femtosecond near ir pulses at a typical laser frequency. We have computed the distribution of the dissociation products between the possible fragmentation channels, their kinetic energy distribution, and the vibrational excitation of the residual molecules using the usual Born-Oppenheimer separation with the two lowest electronic states, thus neglecting the ionization channel. We also make the common assumption that the molecular axes are aligned along the electric field and the rotational motion, which occurs on a much larger time scale compared to the pulse lengths used, can be neglected. In spite of its limitations, this model is of interest for HD^+. It gives a preliminary physical understanding of the branching of the fragments to different channels, with different numbers of absorbed photons, and the role of the permanent dipole moments and nonadiabatic couplings in determining the branching between different ionic states of the dissociation products. This model also helps us to understand the photon absorption pattern at different intensities in terms of evolution of the wave packets in severely distorted and rapidly changing molecular potentials. We have extended our calculation to some regimes of intensity and pulse duration where the results are not expected to be completely realistic. But this extension has enabled us to compare our results with some recent experimental observations and to meaningfully relate those results to our other results, where the assumptions are more acceptable.

II. THEORY

Investigation of photodissociation dynamics of HD^+ within the framework of the BO separation essentially involves the solution of the Schrödinger equation for the nuclear coordinate R in the basis of the two lowest electronic states,

$$i\hbar \frac{\partial \Psi(R,t)}{\partial t} = H(R,t)\Psi(R,t), \tag{1}$$

where

$$H = -\frac{\hbar^2}{2m}\frac{\partial^2}{\partial R^2} + V(R,t), \tag{2}$$

m is the reduced mass of the HD^+ molecule and the potential $V(R,t)$ includes both the interatomic potential and the interaction of the molecule with the laser pulse. This interaction is a function of the nuclear separation R and is given by

$$\tilde{V}(R,t) = \boldsymbol{\mu}(R)\cdot \mathbf{E}(t), \tag{3}$$

where $\boldsymbol{\mu}$ is the dipole moment operator of the molecule operating on the states of nuclear motion through its matrix elements between different electronic states. The BO separation depends on the fact that the motion of the electrons is on a much shorter time scale compared to the time scale of the oscillation of the electronic field vector, $\mathbf{E}$. We also note that the rotational time period of the molecule is orders of magnitude higher than both the pulse time and the characteristic dissociation time, and so we can neglect the rotational degree of freedom. This is a very good approximation and is normally used when femtosecond pulses are involved. The dipole interaction matrix elements with the laser field are taken in the length gauge.

Following the work of Charron *et al.* [23] we have separated all possible states of motion of nuclei within each electronic manifold into two groups (e,o) having even and odd parities, respectively. Thus the radial nuclear wave function has four components, two in each electronic state (G,E) with different parities. The parities of the nuclear wave function arise due to rotation and though rotational motion is neglected, the effective selection rules for radiative coupling are thus taken into account. The radiative interaction couples the components of the wave function with different parities either on the same potential (through the permanent dipole moment operator, $\boldsymbol{\mu}_{GG}$ and $\boldsymbol{\mu}_{EE}$) or on different potentials (through the transition dipole moment operator, $\boldsymbol{\mu}_{GE}$). Thus we have

$$\Psi(R,t) = \begin{pmatrix} \Psi_{G_e}(R,t) \\ \Psi_{G_o}(R,t) \\ \Psi_{E_e}(R,t) \\ \Psi_{E_o}(R,t) \end{pmatrix}. \tag{4}$$

The matrix representation of $V(R,t)$ in the four-component basis is

$$V(R,t)=\begin{pmatrix} V_G(R) & -\boldsymbol{\mu}_{GG}(R)\cdot\mathbf{E}(t) & 0 & -\boldsymbol{\mu}_{EG}(R)\cdot\mathbf{E}(t) \\ -\boldsymbol{\mu}_{GG}(R)\cdot\mathbf{E}(t) & V_G(R) & -\boldsymbol{\mu}_{EG}(R)\cdot\mathbf{E}(t) & 0 \\ 0 & -\boldsymbol{\mu}_{EG}(R)\cdot\mathbf{E}(t) & V_E(R) & -\boldsymbol{\mu}_{GG}(R)\cdot\mathbf{E}(t) \\ -\boldsymbol{\mu}_{EG}(R)\cdot\mathbf{E}(t) & 0 & -\boldsymbol{\mu}_{EE}(R)\cdot\mathbf{E}(t) & V_E(R) \end{pmatrix}. \tag{5}$$

If the initial state is arbitrarily defined to be of even parity, odd (even) parity components of the wave function arise from the net absorption of an odd (even) number of photons. This helps in the interpretation of the dynamics of the system in terms of adiabatic energy curves arising from the interaction of molecular states dressed by different photon numbers. When HD^+ is obtained by ionization of neutral HD, a variety of states with both odd and even parities of nuclear motion can be excited. However, if the gross dynamical features of the dissociation process are not affected by rotational motion, then we can arbitrarily define the initial state to be of either parity. For the alternative choice of the parity of the initial state, the wave packets in the odd and even channels will be interchanged without in any way affecting the final interpretation.

We use the split operator Fourier transform method for solution of the time dependant Schrödinger equation to propagate an initial stationary wave packet on the ground state to a sufficiently large time. Thus the wave packet at a time $t+\Delta t$ can be obtained from the wave packet at time t by the operation

$$\Psi(R,t+\Delta t)=e^{-iH\Delta t/\hbar}\Psi(R,t). \tag{6}$$

The proper Born-Oppenheimer states are the electronic states of H_2^+ with designations $1s\sigma_g$ and $2p\sigma_u$ because the nuclear kinetic energy operator $\partial^2/\partial R^2$ has a diagonal representation in this basis only. However the asymptotic behavior of the fragments is correctly described by the nuclear states whose degeneracy is removed by the incorporation of the nonadiabatic coupling between two asymptotically degenerate nuclear states corresponding to the homonuclear case [24].

At each step of propagation the kinetic energy operator is applied in the basis of the proper Born-Oppenheimer states. The wave-packet components are then transformed to the basis (G,E) with correct asymptotic limits [$D(1s)+H^+$ for G and $H(1s)+D^+$ for E] before applying the operator $V(R,t)$. The wave function components in the basis of the states G and E can be written as [24,25]

$$\Psi_G(\mathbf{r},R)=a(R)\Phi_g(\mathbf{r},R)+b(R)\Phi_e(\mathbf{r},R), \tag{7a}$$

$$\Psi_E(\mathbf{r},R)=-b(R)\Phi_g(\mathbf{r},R)+a(R)\Phi_e(\mathbf{r},R), \tag{7b}$$

where $a(R)$ and $b(R)$ are the mixing coefficients satisfying the normalization condition $a^2(R)+b^2(R)=1$. The potential energies $V_G(R)$ and $V_E(R)$ of two electronic states $\Psi_G(\mathbf{r},R)$ and $\Psi_E(\mathbf{r},R)$, respectively, and the mixing coefficients a and b are taken from the works of Carrington and Kennedy [24] and Moss and Sadler [25].

The dipole moment functions μ_{ug} of H_2^+ are taken from [26] and from these, the matrix elements of transition and permanent dipole moments of HD^+ between the asymptotically correct states are evaluated as follows:

$$\mu_{GE}(R)=\langle\Psi_E(\mathbf{r},R)|-e\mathbf{r}-eR/6|\Psi_G(\mathbf{r},R)\rangle = e[a^2(R)-b^2(R)]\mu_{ug}(R)\approx 0(R\to\infty), \tag{8a}$$

$$\mu_{GG}(R)=\langle\Psi_G(\mathbf{r},R)|-e\mathbf{r}-eR/6|\Psi_G(\mathbf{r},R)\rangle = -eR/6-2a(R)b(R)\mu_{ug}(R)\approx -e2R/3(R\to\infty), \tag{8b}$$

$$\mu_{EE}(R)=\langle\Psi_E(\mathbf{r},R)|-e\mathbf{r}-eR/6|\Psi_E(\mathbf{r},R)\rangle = -eR/6+2a(R)b(R)\mu_{ug}(R)\approx eR/3(R\to\infty). \tag{8c}$$

A distinctive feature of this system is the occurrence of diverging nonzero dipole moment matrix elements between odd and even parity nuclear states of the same electronic state (G or E). These interactions cause redistribution of the particle fluxes between the various photon number channels as shown earlier through time-independent calculations [7]. The influence of these moments on the dynamics has been investigated.

A linearly polarized electric field $E(t)=E_0\cos(\omega t)f(t)\hat{e}$ is used. The pulse shape function $f(t)$ is taken as $\sin^2(\frac{\pi t}{2\sigma})$ with the pulse duration 2σ.

For computing the exponential operator $e^{-iH\Delta t/\hbar}$ involving the sum of the two noncommuting kinetic and potential operators separately, we use the approximation $e^{(A+B)}\sim e^{A/2}e^{B}e^{A/2}$, where A and B are any two noncommuting operators. This method is accurate up to second order. As in [23], the potential matrix is expressed as a linear combination of a diagonal matrix and a number of noncommuting symmetric off diagonal matrices each with two off diagonal elements.

As usual, the exponential of the kinetic energy operator becomes a multiplicative operator with the Fourier transform of the components in the Born-Oppenheimer basis. The wave-packet components are transformed back into the coordinate representation through an inverse Fourier transformation of the coupled state (G,E) basis by Eqs. (7a) and (7b) for application of potential operator. We have adopted the momentum grid rearrangement from Balint-Kurti's program [27] taking the total number of points to be 1024 and we have kept this number the same for both coordinate and momentum representations.

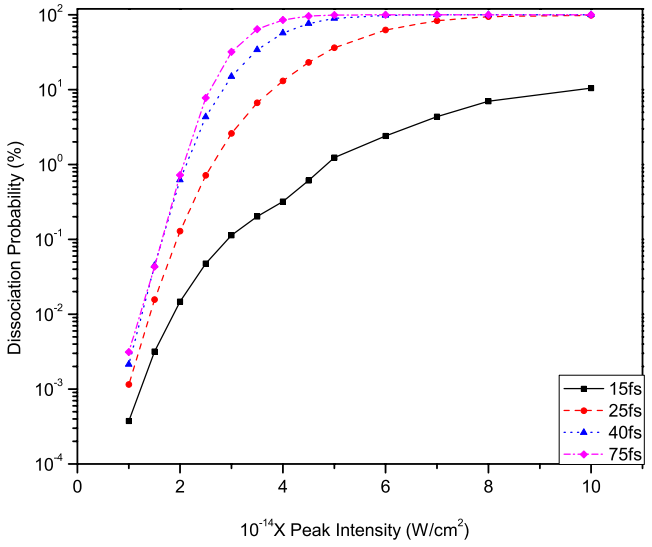

FIG. 1. (Color online) Variation in total dissociation probability with peak intensity for four different pulse durations with wavelength of 800 nm for initial vibrational level $\nu_i=0$.

For finding the energy spectrum of the photofragments, following Heather and Metiu [28], the wave-packet components are expressed as sum of the wave packets in the interaction and asymptotic regions as $\Psi(R,t)=\Psi_I(R,t)+\Psi_A(R,t)$ from the very beginning of its time evolution. The boundary between the two regions is taken to be 40 a.u. Any part of the wave packet crossing the boundary from the interaction region is incorporated in the momentum space representation of the asymptotic part which undergoes a free propagation. This method accurately calculates the kinetic energy spectrum when no significant portion of the wave packet crosses into the asymptotic region during the pulse. The total extent of internuclear distance R is taken to be from 0.2 to 50 a.u. Splitting functions $F(R)=\{1+\exp[c(R-R_0)]\}^{-1}$ and $A(R)=1-F(R)$ are used for smooth transition of the wave packet between the interaction and asymptotic regions with $c=5.0$ $(\text{a.u.})^{-1}$ and $R_0=38.0$ a.u. Use of these parameters gives satisfactory and converged results. The time propagations have been continued up to 50 000 a.u. of time (206.755 ps) during which all parts of the dissociated wave packet reach the asymptotic region and the momentum distribution becomes stable. We have optimized our time grid (Δt) following Kosloff [29] and all results are smoothly converged by taking $\Delta t=0.6$ a.u.

The wave packet in the interaction region is projected on different vibratrional levels of the ground electronic state to get the vibrational distribution of nondissociated molecules.

III. RESULTS AND DISCUSSIONS

Figure 1 shows the total dissociation probability per pulse from the initial state $\nu=0$ for 800 nm $\sin^2$ pulses of four different total pulse durations as functions of peak intensities. This probability is seen to increase steeply with the peak intensity for a fixed pulse duration and with pulse duration when the peak intensity is held fixed. We have continued our calculation to very high intensities in the regime of significant ionization to see how our results compare with some recent experimental data.

For intensities up to about $(5-6)\times10^{14}$ W/cm^2, where dissociation remains the dominant decay mechanism, our one-dimensional (1D) calculation gives very reasonable values for the total dissociation probabilities and the branching between the two ion+atom channels (D+p) and (H+d). Our dissociation probabilities for 15 fs pulses give a remarkable agreement with the two-dimensional (2D) calculation of Roudnev and Esry [21] for a 10 fs full width at half maximum (FWHM) pulse of the same frequency with peak intensities up to 6×10^{14} W/cm^2. For a FWHM of 12.5 fs, somewhat higher than that used by Roudnev and Esry [21] the probabilities in our calculation are higher by a factor of 10–30 in the range of $(2-5)\times10^{14}$ W/cm^2. However, three-dimensional (3D) calculation of Roudnev and Esry [21], going beyond the linear electronic structure, also gives 10–20 times higher probability for a 10 fs FWHM pulse in the range of $(1-3.5)\times10^{14}$ W/cm^2, the proportional increase being higher in the higher intensity range in both calculations. At a higher peak intensity of 7×10^{14} W/cm^2, when ionization becomes important, their 2D calculation gives a dissociation probability of 2.5–2.6% for a 10 fs FWHM pulse while we get 10% probability for a 7.5 fs FWHM pulse of the same peak intensity. The later calculation of Roudnev and Esry [22] gives a probability of about 10% for a 7.1 fs FWHM pulse with peak intensity of 4×10^{14} W/cm^2 while we get a 13% probability with a pulse of 12.5 fs FWHM. Thus our results lie between their 2D and 3D results without the Born-Oppenheimer separation when ionization is unimportant. Just like Roudnev and Esry [22] we get almost the same flux in the H+d and D+p channels (E and G) in all cases. The total dissociation probability for H_2^+, estimated from the kinetic energy distribution patterns in the work of Peng *et al.* [13], is also similar to our calculated results for HD^+ when the same intensity and pulse duration are used. Feuerstein and Thumm [30] also calculated the fragmentation of H_2^+ taking into account the non-Born-Oppenheimer terms through a linear electronic structure. Here also their results qualitatively agree with our calculations for an 800 nm pulse of 25 fs FWHM for $\nu_i=0$ and peak intensity of 2×10^{14} W/cm^2 (0.65%) where the Coulomb explosion channel is not important, as explained in their paper.

We have found that as far the total dissociation probability per pulse is concerned the permanent dipole moments μ_{GG} and μ_{EE} and the nonadiabatic coupling terms, a and b, arising from the breaking of g-u symmetry do not have any effect on the total dissociation probability.

The results of our studies on the effect of these terms on the branching ratio of the dissociation products are summarized in Table I for 800 nm pulses and initial state $\nu_i=0$. From studying the four columns of the table for three different pulse times and two extreme peak intensities, it is clear that for a 25 fs pulse the permanent dipole moments have no influence at all on the distribution of the fragments between the two product channels. However the nonadiabatic couplings tend to equalize them. For shorter pulse times while the pulse is on, the wave packets are confined to a region where the effects of the permanent moments are small. They

TABLE I. Effects of permanent dipole moments and nonadiabatic mixing coefficients on distribution of dissociated photofragments between two channels (G and E) for $\lambda=800$ nm and $\nu_i=0$.

		Branching ratios of dissociated fragments in two channels for $\lambda=800$ nm, $\nu_i=0$ (%)							
		$\mu_{GG}\neq 0$, $\mu_{EE}\neq 0$, a and b are present		$\mu_{GG}=0$, $\mu_{EE}=0$, $a=1$, $b=0$		$\mu_{GG}\neq 0$, $\mu_{EE}\neq 0$, $a=1$, $b=0$		$\mu_{GG}=0$, $\mu_{EE}=0$, a and b are present	
2σ (fs)	I_0 (W/cm^2)	G	E	$G\rightarrow\sigma_g$	$E\rightarrow\sigma_u$	$G\rightarrow\sigma_g$	$E\rightarrow\sigma_u$	G	E
25	10^{14}	50.73	49.27	72.48	27.52	72.47	27.53	50.78	49.22
	5×10^{14}	50.26	49.74	40.88	59.11	40.88	59.11	50.12	49.87
40	10^{14}	54.68	45.31	71.01	28.98	68.95	31.04	54.58	45.41
	5×10^{14}	42.35	57.65	19.71	80.29	20.15	79.84	45.82	54.16
75	10^{14}	50.56	49.43	53.02	46.98	50.80	49.19	52.67	47.33
	5×10^{14}	45.59	54.41	2.17	97.82	47.68	52.21	3.05	96.95

also have lower strengths when the intensity is low enough. The nonadiabatic coupling will cause a sufficiently different distribution from that expected for g-u symmetry only when different components of the wave packet move through the region of this coupling (which increases with R) after the pulse is over. For larger pulse times and higher intensities the wave packet gets sufficient time to reach large distance during the pulse and radiative coupling due to permanent dipole moments (which increase with R) which act for a long time with large strengths, tending to equalize the populations in the two product channels. The symmetry breaking effects are overwhelmed in such cases. Thus redistributions of dissociated molecules between two states are determined by both the nonadiabatic coupling and the permanent dipole moments but differently at different regimes of intensity and pulse length.

Our calculations also give the kinetic energy distributions of the photofragments. As an example, Fig. 2 shows the center of mass kinetic energy distributions of the photrofragments with 75 fs pulses for different peak intensities. At the highest intensity, the three photon and four photon peaks are displaced by about one-photon energy from the expected unperturbed values. Substantial two-photon dissociation is only obtained over a narrow range of intermediate intensities ($\sim 3.5\times10^{14}$ W/cm^2) with kinetic energy shift toward higher values. For other pulse times also the dissociation peak with the minimum number of photon absorption occurs only over a range of intermediate intensities. For shorter pulses the peaks, arising from different numbers of photon absorption, overlap considerably in energy.

In a recent experiment, Orr *et al.* [31] counted the neutral fragments ejected from a cold HD^+ ion beam by an 800 nm laser of 40 fs duration with a peak intensity of 10^{15} W/cm^2 in the direction of polarization for several discrete changes in the time of flight of the neutral fragments from the center of mass system due to kinetic energy released to the dissociation products. They found largest counts in the expected positions for neutral D fragments due to four-photon dissociation, calculated from the unperturbed ground state vibrational energy (4ω peak). In addition, 2ω, 3ω, and 5ω peaks were observed with somewhat lower counts and also weaker 3ω and 4ω peaks for H. Figure 3 shows the plots of squared wave packets in momentum space as functions of the center of mass kinetic energy in the four channels obtained by us for a pulse of 40 fs total duration with the same peak intensity of 10^{15} W/cm^2 and the same central wavelength. The branching ratios are given in Table II. Here the odd or even channel peaks with the kinetic energy expected from two- or three-photon absorption from unperturbed $\nu_i=0$ level are actually generated by net absorption of three or four photons.

Some trends can be clearly established from the reported experimental data without detailed disentanglement of the contribution of various channels. Adjusting the raw data with the calculated shifts of the odd and even peaks (about one-photon redshift) we see that in the experiment [31] about 40% of the dissociation occurs through three-photon absorption in which neutral fragments D and H contribute almost equally. In our calculation we get 70% dissociation through the three-photon absorption channel of which 40% occurs through the neutral H channel. In the experiment, four-photon and five-photon dissociations seem to be almost equal, each contributing 30% of the total dissociation. However, the neutral H channel contributes only about 7–8% in each of these photon absorption channels. The neutral D channel contributes 20–25% in each case. However, in our calculation we could not find signature of any significant dissociation by five-photon absorption. On the other hand, we do get four-photon absorption leading to neutral D and this gives 28% of the total dissociation, in reasonable agreement with the presented experimental data. We get 2% dissociation by four-photon absorption to neutral H, which, though somewhat less than the experimental value, is not grossly different.

This particular aspect of the result is interesting because both in experiment and in our calculation the production of neutral D at the higher energies seems to be favored over the production of neutral H, for similar pulse parameters, though to a smaller extent in the experiment. On the other hand, our calculation does not show such a trend for much shorter and larger pulses (15, 25, and 75 fs) and at lower intensities. Calculation of Roudnev and Esry [21] also gives similar velocity distribution for both neutral and ionized fragments for very short pulses with high intensities (10 fs pulse with a

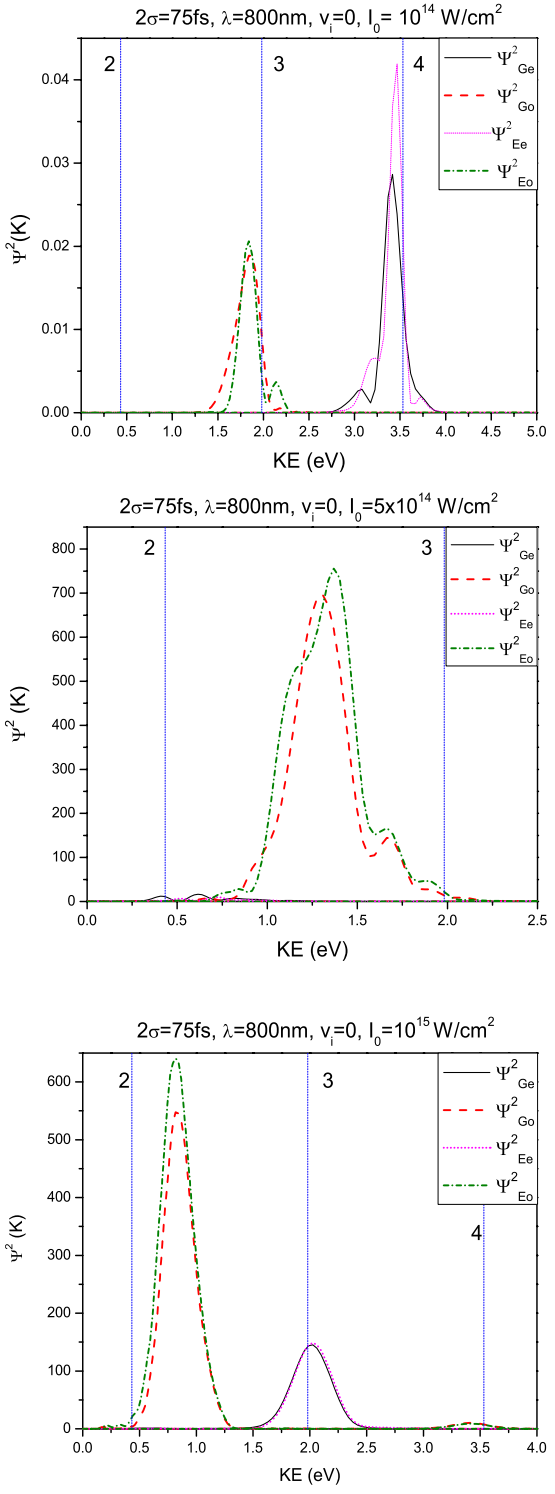

FIG. 2. (Color online) Kinetic energy distribution of dissociated fragments for 75 fs pulse of three different peak intensities.

peak of 7×10^{14} W/cm^2). Thus preponderance of neutral D over neutral H at high kinetic energies corresponding to four-photon absorption occurs only with intermediate duration pulses and increases with intensity. This feature is determined by the motion of the different components of wave packets during the pulse. Our computation demonstrates that for intermediate pulse times as the intensity increases, only

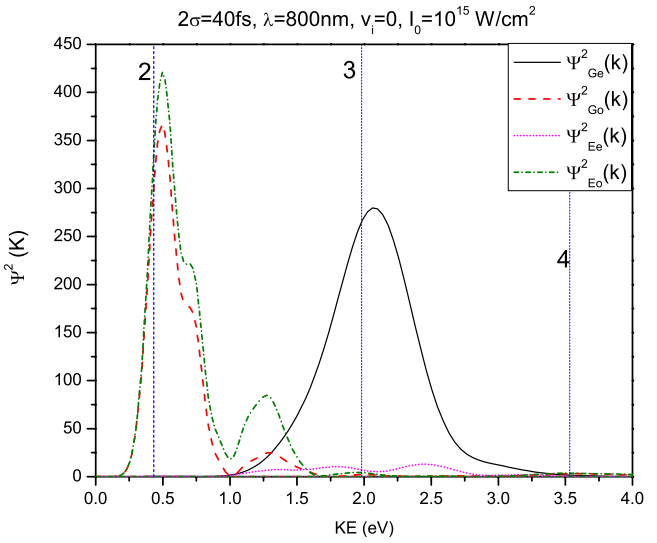

FIG. 3. (Color online) Kinetic energy distribution of dissociated fragments for 40 fs pulse with peak intensity of 10^{15} W/cm^2 and wavelength of 800 nm.

the component with an even G character is accelerated and moves to large R during the pulse and no further transition takes place. This has been discussed in [8]. For other cases such isolated component at large distances are not found.

A qualitative understanding of the branching ratio of the photofragments to different absorbed photon number channels can be obtained by looking at the adiabatic potential curves drawn with the central frequency only and changing with time. Figure 4 shows the adiabatic potential curves for three different intensities along with the diabatic potentials dressed by various numbers of absorbed photons. We note that adiabatic curves are considerably more complex than those usually drawn. This is because at high intensities and the frequency used, the n photon couplings cannot be isolated and their effects on the adiabatic potentials overlap throughout an extended region. We have used an exponential cutoff for the dipole moments beyond $R=R_{\mathrm{cut}}=5$ a.u. so that the curves converge with the dressed diabatic ones at the proper asymptotic limit. Also for short pulses, when the wave packet reaches large values of R, the intensity will start falling so that the adiabatic potential experienced by the packet as it progresses toward large R would certainly tend toward the field free potential.

It is clear that for a peak intensity of 10^{14} W/cm^2 only small portions of the wave-packet tail can be released into the continuum through the five photon avoided crossing (A) at a time only when the intensity approaches its peak value. However, near the six-photon crossing (B) at $R=2.4$ a.u., where the gap is smaller, the initial wave packet tends to have a larger magnitude, and portions of the wave packet released through this path may end up with a net four-photon absorption. Thus for a peak intensity of 10^{14} W/cm^2 there will be competition between net three- and four-photon dissociations. This is clearly seen from Table II which gives the branching ratio between even and odd components of the wave packet in the asymptotic region. This even or odd ratio increases as the pulse time is increased reflecting the impor-

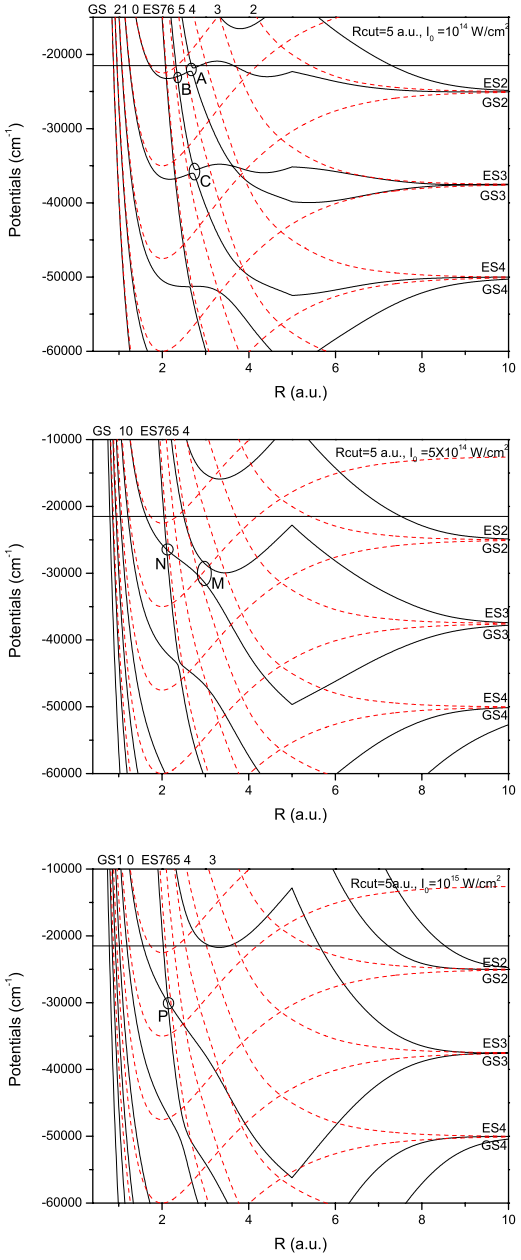

FIG. 4. (Color online) Several relevant adiabatic (solid lines) and dressed diabatic (dashed lines) potentials for HD^+ in a laser field with wavelength of 800 nm for three different intensities. At large and small internuclear separations the number of absorbed photons dressing the diabatic potentials has been indicated for several curves. The horizontal solid line indicates unperturbed ground vibrational level ($\nu=0$).

tance of the next crossing (C) where a diabatic path to the four-photon channel tends to be followed if the intensity falls fast enough. This picture can be confirmed by plotting the magnitude of the wave packets in all the four channels against R at various times for different pulses.

At a higher peak intensity of 5×10^{14} W/cm^2 the avoided crossing at $R=2.9$ a.u. (M) would lead to a three-photon absorption. The seven-photon crossing at $R=2.1$ a.u. (N) is not appreciably opened up to allow adiabatic passage through this crossing to the final four-photon absorption channel. Table II shows that the odd component has a larger norm in the asymptotic region. However there is an appreciable magnitude of the even component at this intensity which seems to arise from a net two-photon absorption particularly at shorter pulse times. This may be caused by trapping of a portion of the wave packet in the well during the rising pulse and its later release into the continuum. The kinetic energy is increased in the process.

Finally, it is seen that at the highest intensity the competition between the diabatic and adiabatic paths at the seven-photon avoided crossing (P) would lead to both three- and four-photon dissociations. For large pulse time the three-photon dissociation channel has a larger contribution because during the rising portion of the pulse, when the seven-photon gap has not sufficiently opened up, but the adiabatic curves are well separated at larger distances, the wave packet gets enough time to escape through the diabatic path at this crossing point and end up in the net three-photon channel by adiabatic passage.

IV. CONCLUSION

Our 1D wave-packet calculations for the dissociation of HD^+ by 800 nm femtosecond pulses with peak intensities of 10^{14}–10^{15} W/cm^2 and four different durations (15, 25, 40, and 75 fs) give the dissociation probability per pulse, the branching ratio of two asymptotic product channels, and the kinetic energy distributions of the fragments in each channel. The vibrational distributions of the nondissociated molecules after the pulse can also be obtained.

The role of Coulomb explosion at the higher intensities cannot be assessed with the present model, but our calculations provide qualitative but convincing agreement with results from more sophisticated models, where simple dissociation is not overwhelmed by Coulomb explosion processes.

The present study nicely illustrates the gradual downward shift through the shift of the fragment energy peaks to lower values. Further, the broadening of each peak as the pulse time is decreased due to the increased bandwidth of the laser field also becomes apparent.

The peaks in the kinetic energy distributions of photofragments can be identified as arising from the net absorption of a particular number of photons. This allows a preliminary comparison with experimental data for branching of the different fragments to different photon absorption channels obtained with vibrationally cold molecules. Indications of the above threshold dissociation process at the higher intensities are thus obtained in agreement with recent experimental works.

The effect of both permanent dipole moments and the nonadiabatic coupling between Born-Oppenheimer states on the dissociation dynamics have been investigated and the results show that the permanent dipole moments change the dissociation branching ratios between the two outgoing channels significantly at large intensities and pulse times. For short pulses and low intensities the nonadiabatic coupling plays a determining role as far as the branching ratios of the dissociation products are concerned.

Our study seems to indicate, in agreement with other calculations, that in general the ratio of total H/D production

TABLE II. Branching ratios of dissociated photofragments for three different pulse durations and four peak intensities.

2σ (fs)	I_0 (W/cm^2)	Branching ratios of dissociated fragments (%)			
		G_e	G_o	E_e	E_o
25	10^{14}	37.30	13.43	35.29	13.98
	3.5×10^{14}	30.44	20.33	27.91	21.31
	5×10^{14}	21.21	29.05	19.66	30.08
	10^{15}	26.06	24.79	23.96	25.17
40	10^{14}	44.86	9.83	26.02	19.29
	3.5×10^{14}	33.08	16.89	30.68	19.41
	5×10^{14}	10.18	32.17	9.53	48.12
	10^{15}	27.66	30.76	1.98	39.58
75	10^{14}	24.07	26.49	27.85	21.58
	3.5×10^{14}	37.35	13.97	25.98	22.69
	5×10^{14}	1.35	44.24	0.83	53.58
	10^{15}	7.90	37.47	7.98	46.64

would be nearly 1. There may be some small deviations at the highest intensities but we were unable to find any precise condition which can lead to a far from 50:50 H/D branching ratio in single frequency strong field photodissociation. However, the energy distribution of the neutral H and D fragments can sometimes be very different, particularly at high intensities and intermediate pulse times. This can be justified from the picture of the spatial propagation but perhaps is not predictable from some general theoretical consideration.

We have also demonstrated how to interpret our results for branching to different photon absorption channels for different intensities and pulse durations using the temporally changing full adiabatic potentials.

[1] X. He, O. Atabek, and A. Giusti-Suzor, Phys. Rev. A **38**, 5586 (1988).
[2] A. Giusti-Suzor, X. He, O. Atabek, and F. H. Mies, Phys. Rev. Lett. **64**, 515 (1990).
[3] A. Giusti-Suzor and F. H. Mies, Phys. Rev. Lett. **68**, 3869 (1992).
[4] E. Charron, A. Giusti-Suzor, and F. H. Mies, Phys. Rev. A **49**, R641 (1994).
[5] L. J. Frasinski, J. Plumridge, J. H. Posthumus, K. Codling, P. F. Taday, E. J. Divall, and A. J. Langley, Phys. Rev. Lett. **86**, 2541 (2001).
[6] A. Giusti-Suzor, F. H. Mies, L. F. DiMauro, E. Charron, and B. Yang, J. Phys. B **28**, 309 (1995).
[7] A. Datta, S. Saha, and S. S. Bhattacharyya, J. Phys. B **30**, 5737 (1997).
[8] J. H. Posthumus, Rep. Prog. Phys. **67**, 623 (2004).
[9] *Molecules in Intense Laser Fields*, edited by A. D. Bandrauk (Dekker, New York, 1994), Chaps. 2 and 3.
[10] H. G. Muller, in *Coherence Phenomena in Atoms and Molecules in Laser Fields*, NATO Advanced Studies Institute, Series B: Physics, edited by A. D. Bandrauk and S. C. Wallace (Plenum, New York, 1992), Vol. 287, p. 89.
[11] G. Jolicard and O. Atabek, Phys. Rev. A **46**, 5845 (1992); O. Atabek and G. Jolicard, *ibid.* **49**, 1186 (1994).
[12] C. Lefebvre, T. T. Nguyen-Dang, and O. Atabek, Phys. Rev. A **75**, 023404 (2007).
[13] L. Y. Peng, I. D. Williams, and J. F. McCann, J. Phys. B **38**, 1727 (2005).
[14] K. C. Kulander, F. H. Mies, and K. J. Schafer, Phys. Rev. A **53**, 2562 (1996).
[15] B. Rotenberg, R. Taïeb, V. Véniard, and A. Maquet, J. Phys. B **35**, L397 (2002).
[16] G. L. V. Steeg, K. Bartschat, and I. Bray, J. Phys. B **36**, 3325 (2003).
[17] V. Serov, A. Keller, O. Atabek, H. Figger, and D. Pavicic, Phys. Rev. A **72**, 033413 (2005); V. N. Serov, A. Keller, O. Atabek, and N. Billy, *ibid.* **68**, 053401 (2003).
[18] E. Charron, A. Giusti-Suzor, and Frederick H. Mies, Phys. Rev. Lett. **75**, 2815 (1995).
[19] A. Datta, S. Saha, and S. S. Bhattacharyya, Phys. Rev. A **60**, 1324 (1999).
[20] V. Roudnev, B. D. Esry, and I. Ben-Itzhak, Phys. Rev. Lett. **93**, 163601 (2004).
[21] V. Roudnev and B. D. Esry, Phys. Rev. A **71**, 013411 (2005).
[22] V. Roudnev and B. D. Esry, Phys. Rev. A **76**, 023403 (2007).
[23] E. Charron, A. Giusti-Suzor, and F. H. Mies, J. Chem. Phys. **103**, 7359 (1995).
[24] A. Carrington and R. Kennedy, Mol. Phys. **56**, 935 (1985).
[25] R. E. Moss and I. A. Sadler, Mol. Phys. **61**, 905 (1987).
[26] D. R. Bates, J. Chem. Phys. **19**, 1122 (1951).

[27] G. Balint-Kurti, www.chm.bris.ac.uk/pt/ggbk/gabriel.htm
[28] R. Heather and H. Metiu, J. Chem. Phys. **86**, 5009 (1987).
[29] R. Kosloff, J. Phys. Chem. **92**, 2087 (1988).
[30] B. Feuerstein and Uwe Thumm, Phys. Rev. A **67**, 043405 (2003).
[31] P. A. Orr, I. D. Williams, J. B. Greenwood, I. C. E. Turcu, W. A. Bryan, J. Pedregosa-Gutierrez, and C. W. Walter, Phys. Rev. Lett. **98**, 163001 (2007).